Physical parameterisation of 3C- Silicon Carbide (SiC) with scope to evaluate the suitability of the material for power diodes as an alternative to 4H-SiC

A. Arvanitopoulos ; N. Lophitis ; S. Perkins ; K. N. Gyftakis ; M. Belanche Guadas ; M. Antoniou

Original citation:
Arvanitopoulos, A; Lophitis, N; Perkins, S; Gyftrakis, K.N; Belanche Guadas, M; Antoniou. M. (2017) Physical parameterisation of 3C- Silicon Carbide (SiC) with scope to evaluate the suitability of the material for power diodes as an alternative to 4H-SiC. *IEEE International Symposium on Diagnostics for Electric Machines, Power Electronics and Drives*, 565-571. ISBN 978-1-5090-0409-6. DOI: 10.1109/DEMPED.2017.8062411

http://dx.doi.org/10.1109/DEMPED.2017.8062411

IEEE

Physical parameterisation of 3C- Silicon Carbide (SiC) with scope to evaluate the suitability of the material for power diodes as an alternative to 4H-SiC

A. Arvanitopoulos, N. Lophitis, S. Perkins, K. N. Gyftakis
Faculty of Engineering, Environment and Computing,
Coventry University, Coventry, UK
arvanita@uni.coventry.ac.uk

M. Belanche Guadas
School of Industrial Engineering,
Polytechnic University of Valencia,
Valencia, Spain

M. Antoniou
Electrical Engineering, University of Cambridge, Cambridge, UK

***Abstract*— Major recent developments in growth expertise related to the cubic polytype of Silicon Carbide, the 3C-SiC, coupled with its remarkable physical properties and the low fabrication cost, suggest that within the next five years, 3C-SiC devices can become a commercial reality. It is therefore important to develop Finite Element Method (FEM) techniques and models for accurate device simulation. Furthermore, it is also needed to perform an exhaustive simulation investigation with scope to identify which family of devices, which voltage class and for which applications this polytype is suited. In this paper, we present a complete set of physical models and material parameters for bulk 3C-SiC aiming Technology Computer Aided Design (TCAD) tools. These are compared with those of 4H-SiC, the most well developed polytype of SiC. Thereafter, the newly developed material parameters are used to assess 3C- and 4H-SiC vertical power diodes, P-i-N and Schottky Barrier Diodes (SBDs), to create trade-off maps relating the on-state voltage drop and the blocking capability. Depending on the operation requirements imposed by the application, the developed trade-off maps set the boundary of the realm for those two polytypes. It also allows us to predict which applications will benefit from an electrically graded 3C-SiC power diodes.**

Keywords*— *3C-SiC, FEM simulations, TCAD model, material parameters, semiconductor physics, vertical diodes, SBD, P-i-N.

I. INTRODUCTION

Wide bandgap semiconductors have advanced electrical characteristics compared to silicon (Si), which means they can induce a step improvement for power converter systems. During the past decade, there has been a remarkable effort to overcome issues related to the reliability of 4H-SiC devices in particular. As a result, a number of devices are now readily available in the market. Schottky Barrier Diodes (SBDs) with blocking voltages of 600–1700 V are now commercially available and have already demonstrated substantial reduction of power loss in various power conversion systems [1]. At the same time, the interest for high voltage power rectifiers has led to the design of SiC Schottky diodes blocking voltages of as high as 15 kV [2]. However, the resulted degraded material quality and limitations induced by current packaging technology hindered their suitability for use in commercial applications. It is however important to stress the significant progress achieved in this area. This includes the fabrication of Schottky diodes rated for 4.9 kV [3]. Higher-voltage, up to 6.5 kV, SiC majority carrier devices have also been demonstrated [4] [5]. Bipolar switches are preferred in high voltage applications to keep the on-losses low. According to [6] the boundary between unipolar and bipolar devices is located at 3 kV–6 kV in the case of SiC technology. A P-i-N rectifier based on 4H-SiC semiconductor technology with breakdown voltage of 8.6 kV is discussed in [3]. Further, the fabrication and characterization of 6 kV and 10 kV rated P-i-N devices is studied in [7].

There are no 3C-SiC devices available for commercial use. However, there is an increase, in the community that focuses in making the necessary improvements, in the processes that relate to the material development that could soon allow that. Although there are published works in literature denoting the interest of modelling 3C-SiC power devices [8] [9] and simulating [10] [11] with Monte Carlo method, yet, to the best of the authors knowledge, no reports on the complete parametrization of the cubic SiC polytype for accurate FEM analysis are present. Taking into consideration that this certain semiconductor technology is in a constant development process, the absence of the material parameter information inhibits the capability to investigate 3C-SiC power devices. This work has the prospect of offering an initial global baseline for TCAD physical modelling of the 3C-SiC compound semiconductor. Thus, performance optimization of the cubic silicon carbide power devices, along with performance comparisons to other technologies, can be achieved. The fact that no 3C-SiC wafers are yet commercially available [12], it enhances the importance of this effort.

Moreover, the application requirements for power devices characterized by higher blocking voltages are usually met using long drift regions to keep the electric field moderate in reverse operation, in the cost of increasing the on-state loses. The investigated TCAD physical model of 3C-SiC technology is compared to the market favorite, 4H-SiC at device level. The aim of this work is to provide a map in deciding which power diode technology suits better each application needs, depending

978-1-5090-0409-6/17/$31.00 ©2017 IEEE

on the demands of forward voltage drop and blocking capabilities in the range of 200 V up to 6.5 kV.

The remaining part of this work is organized as follows. In section II, the parameter file of 3C-SiC is structured for TCAD tools. In section III, 3C-SiC power diodes are compared to 4H-SiC in terms of breakdown voltage and on-state voltage drop. Finally, in section IV the conclusions are presented.

II. Physical Modelling of 3C-SiC

In the following sub-sections we discuss the parameter sets that fully describe the 3C-SiC compound semiconductor allowing for TCAD simulations. The discussion is mainly on coefficient values of this material as found in literature studies so far. The corresponding values of the already existing and well-studied parameter file for 4H-SiC are also presented for direct comparison purposes. Further, each physical mechanism presented is accompanied with the corresponding identified limitations.

A. Bandgap parameters for 3C-SiC

TCAD tools model the lattice temperature dependence of the band gap as described in (1), where $E_g(0)$ is the band gap energy at 0 Kelvin and α, β are material parameters [13].

$$E_g(T) = E_g(0) - \alpha T^2/(T+\beta) \quad (1)$$

The 3C-SiC is an indirect bandgap semiconductor and the energy band gap is defined as the minimum distance of maximum valence band (Γ15) to minimum conduction band (X1C) resulting in $\Gamma_{15}^{u} - X_1^c = 2.39eV$. The electron affinity is the energy separation between the conduction band and the vacuum and can be considered as well as temperature dependent affected by bandgap narrowing. Considering bandgap narrowing splitting equally between conduction and valence bands, the parameter 'Bgn2Chi' in Table I, is set to the 0.5 value. The main difference of the bandgap models is how they handle bandgap narrowing (2).

Table I: 3C-SiC parameter set related to Bandgap.

Parameters Description	Parameter Name	3C-SiC	4H-SiC
Electron affinity (eV)	*Chi0*	*3.83*	*3.24*
Bandgap narrowing coefficient	*Bgn2Chi*	*0.5*	*0.5*
$E_g(0)$ [eV]	*Eg0*	*2.39*	*3.29*
α	*alpha*	*6x10^{-3}*	*3.3x10^{-2}*
β	*beta*	*1200*	*1x10^{5}*

$$E_{bgn} = \Delta E_g^0 + \Delta E_g^{Fermi} \quad (2)$$

where ΔE_g^0 is determined by the particular bandgap narrowing model used, and ΔE_g^{Fermi} is an optional correction to account for carrier statistics. In this work we consider Maxwell–Boltzmann statistics when investigating the dynamics of a collection of carriers. For power devices that their size is relatively large, compared to the de Broglie wavelength of electrons, this is a quite good approach. Thus, it is safe to assume that this correction term is negligible. According to (1) and the theoretical analysis in [14] the parameter set for the bandgap of 3C-SiC semiconductor material is summarized in Table I. The value of energy band gap for 3C-SiC is smaller compared to that of 4H-SiC, which in turn causes a lower critical field value.

According to [15], power devices that contain layers with different doping profiles may affect their behavior by leading to band-edge displacements. These displacements representing potential barriers, influence carrier transport phenomena in the device and their interactions. Lindefelt [15] proposes a model for the band-edge displacements of n-type 3C-SiC material, valid for majority carriers concentrations typically above $10^{18}cm^{-3}$. This model essentially constitutes an extension of the Jain-Roulston (J-R) theory [16] implemented in TCAD tools for describing the bandgap narrowing dependence on doping concentration. In (3) the A, B, C, and D are material dependent coefficients.

$$\Delta E_g^0 = A \cdot N_{tot}^{1/3} + B \cdot N_{tot}^{1/4} + C \cdot N_{tot}^{1/2} + D \cdot N_{tot}^{1/2} \quad (3)$$

The values of these coefficients for the 3C-SiC occur after some basic computation on the values determined in [15]. This is a necessary step in order to have the parameters in the appropriate form needed to be utilized by J-R model in (3).

In addition, from [14] [17], the static dielectric constant of the cubic SiC is defined as $\varepsilon_0^{3C} = 9.72$ whereas for 4H-SiC is $\varepsilon_0^{4H} = 9.66$.

Table II: 3C-SiC band gap narrowing doping dependence.

Lindefelt model coefficients	3C-SiC semiconductor material	
	n-type	***p-type***
A	*-1.48x10^{-8}*	*1.3x10^{-8}*
B	*1.75x10^{-7}*	*-1.5x10^{-7}*
C	*-3.06x10^{-12}*	*1.43x10^{-12}*
D	*6.85x10^{-12}*	*-6.41x10^{-13}*

B. Density of States in conduction and valence band

According to literature, computing the effective carrier mass as a function of temperature-dependent Density of States (DoS) is an option that best suits the parameters for 3C-SiC. Thus, taking into account the work in [18], the (4) can be utilized.

$$N_C(T) = 4.82 \cdot 10^{15} \cdot M \cdot (m_c/m_0)^{3/2} \cdot T^{3/2}(cm^{-3}) \quad (4)$$

$$N_V(T) = 2.23 \cdot 10^{15} \cdot T^{3/2}(cm^{-3}) \quad (5)$$

$$n_i(T) = \sqrt{N_C N_V} exp\left(-E_g/2kT\right) \quad (6)$$

where, $M = 3$ the number of equivalent valleys in the conduction band, $m_c = 0.35m_0$ the effective mass of the density of states in one valley of conduction band, $m_{cd} = 0.72m_0$ the effective mass of density of states. In the same sense we exploit the expression from [19] and [20] to get (5). The parameter values for this set are summarized in Table III, as acquired from the aforementioned literature sources. Further, the intrinsic carrier concentration (n_i) expressed in (6), is determined by the thermal generation of electron-hole pairs

across the energy bandgap [20] [21]. Thus, the wide bandgap 4H-SiC, having lower intrinsic carrier concentration, can maintain semiconductor characteristics at much higher temperature than 3C-SiC semiconductor.

Table III: 3C-SiC temperature dependent Density of States.

Parameters Description	Parameter Name	3C-SiC	4H-SiC
N_C (300K)	*Nc300*	*1.559x10^{19}*	*1.719x10^{19}*
N_V (300K)	*Nv300*	*1.159x10^{19}*	*2.509x10^{19}*
Intrinsic carrier concentration [cm^{-3}]	n_i	*0.83x10^{1}*	*5.64x10^{-9}*

C. *Mobility mechanisms and dependences*

In TCAD simulations the most frequently used model to describe the doping dependence of carriers mobility in the semiconductor is the Masetti model. The Caughey – Thomas (C-T) expression [22] approximates this model and can be utilized in order to determine the mobility doping dependence parameters under low applied field conditions. The C-T formula is shown in (7) where, N is the total doping concentration, μ_{max} is the mobility of undoped or unintentionally doped samples, μ_{min} is the mobility in highly doped material, N_{ref} is the doping concentration at which the mobility is halfway between its minimum and maximum value and α is a measure of how quickly the mobility changes in this range. However, in [23] it is stated that this model fails for the case of 3C-SiC as there does not appear to be a definite value for μ_{min}. Thus a model that behaves like the C-T expression for low doping and like Powel's [24] for high doping is proposed.

In this work, the authors target to investigate the behavior of 3C-SiC power diodes that include junctions formed between regions lightly or heavily doped. As a consequence, the doping effect on carrier mobility is important. Experimental data available in [23] are employed and various values for the minimum mobility are investigated utilizing the C-T expression. For doping concentrations ranging from $10^{14} - 10^{21}\ cm^{-3}$, a minimum mobility value of $40\ cm^2/Vs$ is determined approximately [20], as shown in Fig. 1.

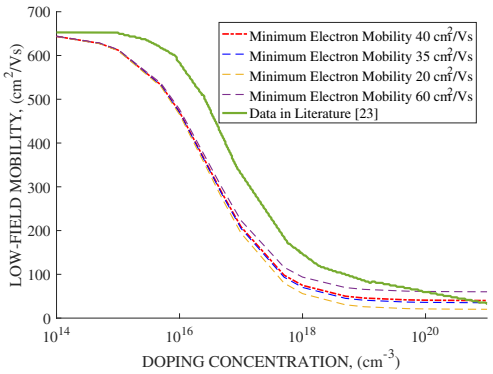

Fig. 1. The minimum mobility value of 3C-SiC is defined in [20] at $40\ cm^2/Vs$. Adopting this value, a good approximation of the material low-field mobility can occur.

Moreover, the Fermi level measured from the conduction band changes with temperature and so do all the parameters involved in the mobility description. The temperature dependence for the low-field mobility parameters is described by (8), where Par is the parameter of interest from (7) and Par_0 is the value of the parameter at 300 Kelvin.

$$\mu_{low} = \mu_{min} + (\mu_{max} - \mu_{min})/\left(1 + \left(N/N_{ref}\right)^{\alpha}\right) \quad (7)$$

$$Par = Par_0 \cdot (T/300)^{\gamma} \quad (8)$$

The 3C-SiC mobility experimental dataset processed in [25] is exploited by curve fitting of (8) to result in $\gamma_{min} = 0.5$ for the μ_{min} parameter. The electrons' low field mobility parameter values for 3C-SiC are presented in Table IV, as adopted from [23] along with the μ_{min} value obtained from [20]. The corresponding holes' values, supplemented from [18], are also summarized in Table IV. Note that the temperature dependencies omitted for some parameters, are considered to be zero. Taking into account the variance of Fermi level with temperature, presented in [25], the carrier concentration of $1.5x10^{17}cm^{-3}$ is calculated to illustrate the dependence of the mobility at a wide range of temperatures. The results of utilizing the C-T model with the parameter values of Table IV are shown in Fig. 2 and are consistent to the experimentally measured Hall mobility with temperature plotted in [25]. However, a discrepancy can be noticed that becomes more intense when the temperature of the material is around the value of 300K or more. Nevertheless, the parameters presented in this subsection are a good initial approximation for investigating 3C-SiC power devices at a wide operational temperature range.

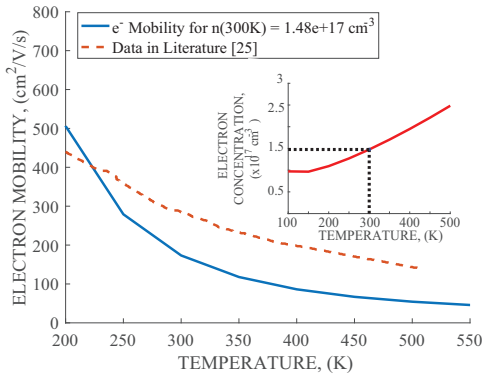

Fig. 2. The low-field mobility of electrons in 3C-SiC dependence on temperature, utilizing the parameters in Table IV, are compared to data in [25]. Both curves correspond to a doping concentration of $1.48x10^{17}cm^{-3}$, as shown in the embedded smaller plot, calculated upon the relative position of the Fermi level that changes with temperature.

Table IV: 3C-SiC parameters for low Field mobility and coefficients used to express temperature dependence.

Parameter	3C-SiC		4H-SiC	
	electrons	***holes***	***electrons***	***holes***
μ_{max} [cm^2/Vs]	*650*	*20*	*950*	*125*
γ_{max}	*-2.5*	*-2.5*	*-2.4*	*-2.15*
μ_{min} [cm^2/Vs]	*40*	*15*	*40*	*15.9*
γ_{min}	*-0.5*	*-0.5*	*-1.536*	*-0.57*
N_{ref} [cm^{-3}]	*3x10^{16}*	*3x10^{16}*	*1.94x10^{17}*	*1.76x10^{19}*
α	*0.8*	*0.8*	*0.61*	*0.34*

For the high field case, the Canali mobility formula is used in TCAD as shown in (9), where E is the electric field strength.

$$\mu(E) = \frac{(\alpha+1)\mu_{low}}{\alpha + \left[1 + \left(\frac{(\alpha+1)\mu_{low}E}{v_{sat}}\right)^{\beta}\right]^{1/\beta}} \quad (9)$$

$$v_{sat} = v_{sat,0}\left(\frac{300}{T}\right)^{v_{sat,exp}} \quad (10)$$

$$v = \frac{v_{sat,n}\mu E}{v_{sat,n} + \mu E} \quad (11)$$

The first parameter to be defined is the one describing the temperature dependence β. Consequently, following the (8), the values of β_0 and γ_β should be determined. In [23], these coefficients are defined by utilizing a model slightly different to this expression. Therefore, in order to make a match, a process was carried out to transfer these parameter values to fit the (8). The results of this process are illustrated in the embedded plot of Fig. 3. Further, according to [26], the nonlinear dependence of the electron drift velocity on electric field for SiC polytypes can be initially approached with the one used for Si-technology, (11), and still be valid. Utilizing all the necessary parameters for mobility from Table IV along with the value of $v_{sat} = 2.5 \times 10^7\ cm/s$ [26] and (11), the parameter $v_{sat,exp}$ from (10) can be easily appraised. The parameters for the high field mobility dependence are assumed to be the same for both carrier types and are summarized in Table V. The red line in the plot of Fig. 3 shows how the model predicts the effect of electric field on the velocity. The parameter values used to produce this plot are those presented in Table V. The dashed line corresponds to the plot of the accurate Monte Carlo simulation results in [27]. Qualitatively, the two lines are of the same shape, however a discrepancy can be observed.

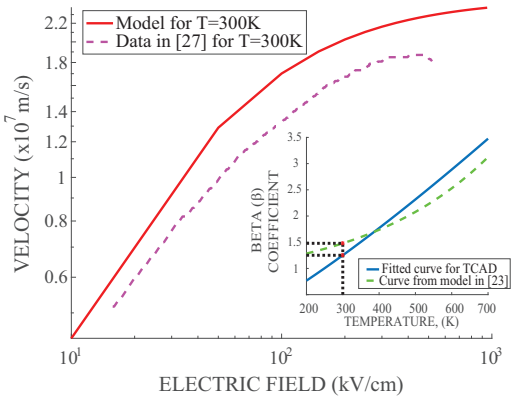

Fig. 3. A comparison of the steady state carriers velocity vs electric field between the high field parameters presented in this work (red line) and the Monte Carlo simulation data available in [27]. The embedded plot presents the transferring of the β_0 and γ_β parameter values from the model in [23] to fit the expression in (8).

Table V: 3C-SiC parameters for high Field mobility and coefficients used to express temperature dependence.

Parameter	3C-SiC		4H-SiC	
	electrons	*holes*	*electrons*	*holes*
β_0	*1.251*	*1.251*	*1.2*	*1.2*
γ_β	*1.2*	*1.2*	*1.0*	*1.0*
v_{sat}	*2.5x10^7*	*2.5x10^7*	*2.2x10^7*	*2.2x10^7*
$v_{sat,exp}$	*1.55*	*1.55*	*0.44*	*0.44*

D. Impact Ionization

The main parameters needed for calculation of the breakdown voltage and critical electric field are ionization coefficients of electron and holes, which are considered constant and material dependent. It is found, in [28], that the impact ionization coefficients of bulk 3C-SiC are relatively insensitive to temperature variations in the range of $300K < T < 500K$. In TCAD tools the "van Overstraeten de Man" model [29] [30] can be used for impact ionization. Regarding 3C-SiC, ionization coefficients have been determined for holes and there is the assumption that they are the same for electrons [31]. Following the (12) and (13), the ionization coefficients for electrons and holes at room temperature for 3C-SiC are adopted and summarized in Table VI [32]. The factor γ with the optical phonon energy $\hbar\omega_{op}$ expresses the temperature dependence of the phonon gas against which carriers are accelerated, where $T_0 = 300K$ and F_{ava} the driving force for impact ionization, namely the applied electric field on the power device.

Table VI: 3C-SiC impact ionization coefficients.

Parameters Description	Parameter Name	3C-SiC
Ionization coefficients for electrons and holes	$a_{n,p}$	*1.07x10^7*
	$b_{n,p}$	*1.12x10^7*
Low field range up to this value	E_0	*4x10^5*
Optical phonon energy	$\hbar\omega_{op}$	*0.120*
		0.098

$$\gamma = \frac{\tanh\left(\hbar\omega_{op}/2kT_0\right)}{\tanh\left(\hbar\omega_{op}/2kT\right)} \quad (12)$$

$$\alpha(F_{ava}) = \gamma\alpha exp(-\gamma b/F_{ava}) \quad (13)$$

E. Incomplete Ionization

In TCAD tools, the phenomenon of incomplete ionization can be included by implementing traps. Depending on the dopant solubility in the semiconductor, various shallow energy levels are formed. These shallow defects in the semiconductor affect the Fermi-level and describe the available charge carriers needed for conductivity [33]. Following the published works in [34], [35], [36], [37] and [38], we come up with the values of Table VII, that presents the main impurities in 3C-SiC material due to different specific donor and/or acceptor species.

Table VII: 3C-SiC impurities / Shallow traps due to doping.

Impurity	Species Type	Energy Levels (eV)	
		3C-SiC	*4H-SiC*
Nitrogen	donor [a]	*0.057*	0.071
Vanadium	donor [a]	*0.660*	0.800
Aluminum	acceptor [b]	*0.260*	0.265
Gallium	acceptor [b]	*0.343*	0.300
Boron	acceptor [b]	*0.735*	0.293

[a] The formed energy level is considered from the Conduction band (E_C).

[b] The formed energy level is considered from the Valence band (E_V).

F. Auger Recombination in 3C-SiC

The Auger mechanism is used to describe the band-to-band non-radiative recombination, namely the process that includes the emission of a phonon. The band-to-band Auger recombination rate in (14) decreases with increasing carrier density because of the screening Coulomb interaction [39]. The

Auger recombination rate is found to be an order of magnitude lower in 3C-SiC with respect to 4H-SiC, as can be seen in Table VIII.

$$R_{net}^{A} = \left(C_n n + C_p p\right)\left(np - n_{i,eff}^2\right) \quad (14)$$

According to [39], it is safe to assume that in 3C-SiC the temperature dependence and the influence due to different carrier concentrations of Auger recombination coefficient is negligible. Therefore, constant values are adopted for each carrier type, as defined in [39], and shown in Table VIII.

Table VIII: 3C-SiC Auger recombination rates.

Parameter	3C-SiC	4H-SiC
Electron coefficient (C_n)	$0.3x10^{-31}$	$5x10^{-31}$
Holes coefficient (C_p)	$0.2x10^{-31}$	$2x10^{-31}$

G. Schockley-Read-Hall (SRH) Recombination

Generation and recombination mechanisms, are very important in power device physics, in particular, for bipolar devices. The SRH expression describes these recombination processes, that are considered dominant for semiconductors with indirect bandgap [40], as can be seen in (15).

$$R_{net}^{SRH} = \frac{np - n_i^2}{\tau_p(n + n_1) + \tau_n(p + p_1)} \quad (15)$$

$$\tau_{dop} = \tau_{min} + \frac{\tau_{max} - \tau_{min}}{1 + \left(\frac{N_{A,0} + N_{D,0}}{N_{ref}}\right)^{\gamma}} \quad (16)$$

Table IX: 3C-SiC SRH lifetimes parameter set.

Parameter	3C-SiC		4H-SiC	
	electrons	*holes*	*electrons*	*holes*
τ_{min} [sec]	*0*	*0*	*0*	*0*
τ_{max} [sec]	$2.5x10^{-6}$	$0.5x10^{-6}$	$2.5x10^{-6}$	$0.5x10^{-6}$
N_{ref} [cm^{-3}]	$1x10^{17}$	$1x10^{17}$	$3x10^{17}$	$3x10^{17}$
γ	*0.3*	*0.3*	*0.3*	*0.3*

The doping dependence of the SRH lifetimes is modelled with the Scharfetter relation shown in (16). Carrier's lifetime vary in literature for 3C- with best reported measured values of 10-15μs [41]. Additionally, authors in [42] claim lifetime values equal to 0.5μs, though without specifying the corresponding doping concentration. These values are strongly dependent on the quality of each unique heteroepitaxially grown material layer and are expected to lower due to electrical active traps. Hence we adopt the values existing for 4H technology, as in all sources they are approximately of the same magnitude. Inspecting the values given in [42], lifetime in 3C-SiC is slightly higher than 4H-SiC, thus we determine a lower reference doping concentration (N_{ref}). However, introducing deep levels in the physical model of 3C-SiC will have a great affection on the lifetimes.

III. 3C-SiC vs 4H-SiC Power Diodes Comparison

In this section, results from multiple FEM simulations, utilizing TCAD tools, regarding the I-V characteristics of power diodes, namely Schottky and P-i-N structures, are compared in order to obtain a performance map for each device in respect to the on-state voltage drop. The rated voltage of power devices can be an indication as to which applications can be better served by them. Therefore this map can also be a useful tool when trying to identify whether an application in the market would benefit from the developments on 3C-SiC technology.

In this work, vertical freestanding 3C-SiC power diodes are considered. The material is also considered to have low defects density. Hence, in these devices the doping and thickness of the epitaxial layer essentially determine their resistance and breakdown voltage [3]. Schottky barrier diodes were initially designed for simulations. In this case, the on-state voltage drop is primarily determined by the metal-semiconductor junction barrier height that depends on the workfunction of the metal utilized. For this work, the Schottky contact is assumed to have a workfunction of 5.65eV, which resembles Platinum (Pt) metal. The SiC epitaxial layer thickness considered for the designs, is in the range of 5-100um. The SBDs are designed to be Punch Through (PT) and feature a buffer layer that is 1μm thick. For the PT designs, the electric field distribution in the device is allowed to insert the buffer area and defuse, resulting in a more rectangular shape and thus greater breakdown voltage. On the contrary, due to the absence of the buffer layer, in the NPT design the distribution of the field should not cross the drift region limits, otherwise early breakdown may occur.

When developing 3C-SiC epitaxial layers, the process typically involves a nitrogen rich environment. This unintentionally dopes the grown material epilayers. The current state-of-the-art technology does not allow development of very low concentrations for the SiC drift region. The range of doping concentrations considered for the simulations in this work, range from $9 \times 10^{14}\ cm^{-3}$ up to $1 \times 10^{16}\ cm^{-3}$. This is consistent with the range of values reported in the literature [43].

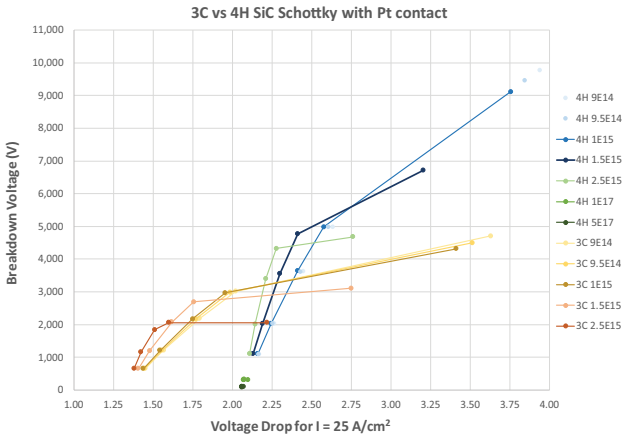

Fig. 4. Breakdown voltage of 3C-SiC and 4H-SiC Schottky power diodes as a function of voltage drop at 25A/cm^2. The equi-doping lines resemble a constant doping concentration for various values of thickness. The left most point in each equi-doping line corresponds to lower drift region thickness value whereas the right most point denotes increased thickness.

Fig. 4, depicts the breakdown voltage of 3C-SiC and 4H-SiC Schottky power diodes as a function of voltage drop at

25A/cm^2. This resembles a low load condition. The 3C-SiC Schottky devices demonstrate lower voltage drop for breakdown voltage application requirements up to 3 kV. For higher blocking capability, the 4H-SiC is preferable as the voltage drop compared to 3C-SiC is lower. Considering higher loads, as shown in Fig. 5, the breakdown boundary changes and becomes 1.8-2 kV.

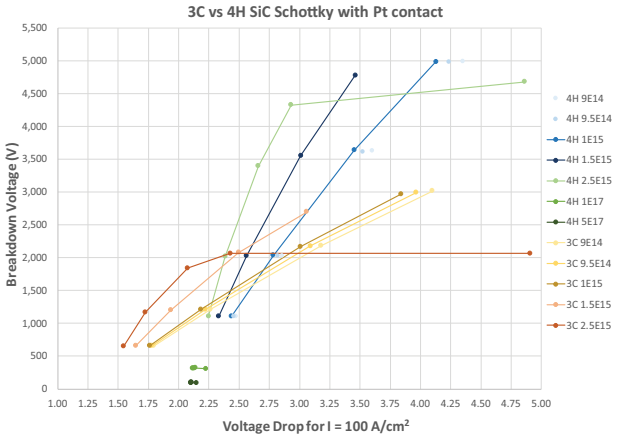

Fig. 5. Breakdown voltage of 3C-SiC and 4H-SiC Schottky power diodes as a function of voltage drop at 100A/cm^2. The equi-doping lines resemble a constant doping concentration for various values of thickness.

A similar methodology was followed with P-i-N diodes. The investigated ranges of drift region doping concentration are $10^{13}\ cm^{-3}$ up to $5 \times 10^{16}\ cm^{-3}$. The drift region thicknesses considered range 5μm to 200μm. The simulation results for 100A/cm^2 load conditions are shown in Fig. 6. As shown, the 3C-SiC is a more attractive solution for power diodes when rated reverse voltages of 200-2200 V are considered. On the other hand, the 4H-SiC P-i-N offers greater blocking capabilities for the same device dimensions in the cost of increased voltage drop during on-state as can be seen in Fig. 6. It should also be noticed that even after deciding in one technology, there still are optimal solutions for some certain values of breakdown voltages, in terms of minimizing the on-state voltage drop by changing the doping concentration and the thickness of the drift region. For the PT design trapezoidal field distribution is supported in the device when blocking. As a result, by increasing the thickness, more voltage can be accommodated within the drift region. However, when the doping concentration is high, the material critical electric field is reached whilst the shape of electric field is still triangular. Consequently, any further increase in the drift length does not improve the breakdown capability. This explains why the equi-doping lines in Fig. 6 stay flat for doping concentrations of $5\times 10^{15}\ cm^{-3}$ or higher after a certain thickness is reached.

The same behavior is noticed for higher application loads in Fig. 7. Assuming that the value of $5\times 10^{15}\ cm^{-3}$ is the normally achievable minimum doping concentration for the drift region, devices with blocking capabilities of more than 1.2 kV cannot be fabricated with 3C-SiC material. Hence, applications requiring more than 1.2 kV should be accommodated by utilizing 4H-SiC power diodes.

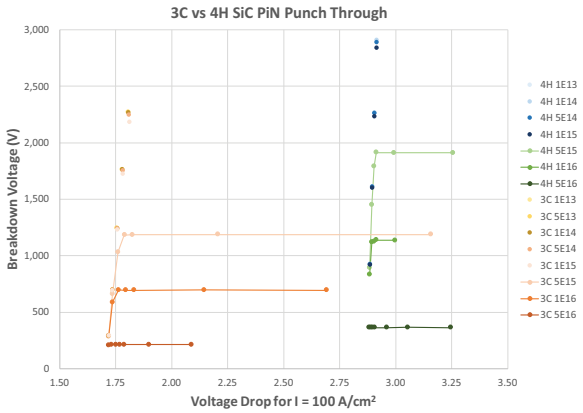

Fig. 6. Breakdown voltage of 3C-SiC and 4H-SiC P-i-N PT power diodes as a function of voltage drop at 100A/cm^2. The equi-doping lines resemble a constant doping concentration for various values of thickness.

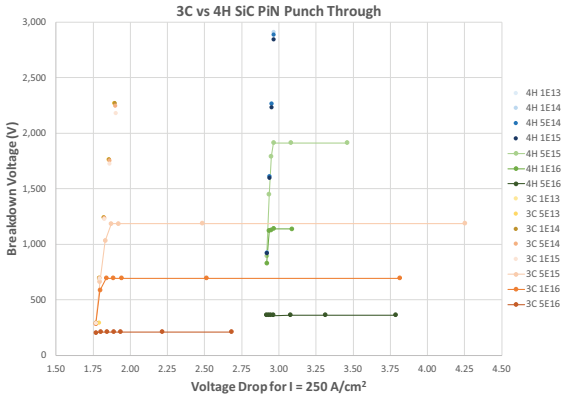

Fig. 7. Breakdown voltage of 3C-SiC and 4H-SiC P-i-N PT power diodes as a function of voltage drop at 250A/cm^2. The equi-doping lines resemble a constant doping concentration for various values of thickness.

IV. Conclusions

In this paper, we present a set of parameters and models that allow TCAD simulation of 3C-SiC devices. This enabled us to successfully model and simulate SBDs and P-i-N structures with 3C-SiC as the material of choice, something that previously was not possible. The parameters used, were mainly adopted unaltered and as published in various sources in the literature. Some basic modifications were also involved, when needed, to fit the available values to the chosen models. As shown, these parameters along with these models give reasonable but not perfect match to published experimental data. Therefore, there exists the imperative need to redefine, fine-tune and revalidate the parameters for even more accurate modelling and simulation of devices. Finally, the inclusion of traps and defects in the 3C-SiC model should also be considered. Indeed, this can allow for a more accurate performance and reliability analysis of real power devices. It can also allow for a physics of failure analysis and the design of devices that can mitigate the effect of these defects. Nevertheless, the performed comparison between the 3C-SiC and the 4H-SiC SBDs and P-i-Ns, allowed us to conclude that 3C-SiC can win over the 4H-SiC for applications requiring up

978-1-5090-0409-6/17/$31.00 ©2017 IEEE

to 1.2 kV blocking voltage, e.g. when used in the automotive industry. The authors aim to define the range of switching frequencies for which this can be achieved by analyzing the switching loses in a future work.

REFERENCES

[1] T. Kimoto, K. Yamada, H. Niwa, and J. Suda, "Promise and Challenges of High-Voltage SiC Bipolar Power Devices," *Energies*, vol. 9, no. 11, p. 908, 2016.

[2] A. K. Agarwal *et al.*, "An overview of SiC power devices," *2010 Int. Conf. Power, Control Embed. Syst.*, pp. 1–4, 2010.

[3] R. Singh, J. A. Cooper, M. R. Melloch, T. P. Chow, and J. W. Palmour, "SiC power Schottky and PiN diodes," *IEEE Trans. Electron Devices*, vol. 49, no. 4, pp. 665–672, 2002.

[4] J. W. Palmour, "Silicon carbide power device development for industrial markets," p. 1.1.1-1.1.8, 2014.

[5] M. Imaizumi and N. Miura, "Characteristics of 600, 1200, and 3300 v planar SiC-MOSFETs for energy conversion applications," *IEEE Trans. Electron Devices*, vol. 62, no. 2, pp. 390–395, 2015.

[6] T. Kimoto, "Material science and device physics in SiC technology for high-voltage power devices of thermal oxidation and hydrogen annealing," *Jpn. J. Appl. Phys.*, vol. 54, 2015.

[7] R. Singh *et al.*, "Large area, ultra-high voltage 4H-SiC p-i-n rectifiers," *IEEE Trans. Electron Devices*, vol. 49, no. 12, pp. 2308–2315, 2002.

[8] F. Li *et al.*, "Study of a novel lateral RESURF 3C-SiC on Si Schottky diode," *2014 16th Eur. Conf. Power Electron. Appl. EPE-ECCE Eur. 2014*, pp. 1–10, 2014.

[9] P. D. Lungu, "Modelling of SiC vertical power DMOSFET structure using the fundamental MOSFET's set of equations," *Int. Semicond. Conf.*, vol. 2, no. 3, pp. 27–30, 1996.

[10] K. F. Brennan *et al.*, "Materials theory based modeling of wide band gap semiconductors: from basic properties to devices," *Solid. State. Electron.*, vol. 44, no. 2, pp. 195–204, Feb. 2000.

[11] Z. Rong, F. Gao, and W. J. Weber, "Monte Carlo simulations of defect recovery within a 10 keV collision cascade in 3C–SiC," *J. Appl. Phys.*, vol. 102, 2007.

[12] A. Stefanskyi, Ł. Starzak, and A. Napieralski, "Silicon Carbide Power Electronics for Electric Vehicles," *2015 Tenth Int. Conf. Ecol. Veh. Renew. Energies*, pp. 1–9, 2015.

[13] W. Bludau and A. Onton, "Temperature dependence of the band gap of silicon," *J. Appl. Phys.*, vol. 45, no. 4, 1974.

[14] K. Rogdakis *et al.*, "Theoretical comparison of 3C-SiC and Si nanowire FETs in ballistic and diffusive regimes," *Nanotechnology*, vol. 18, no. 47, p. 475715, 2007.

[15] U. Lindefelt, "Doping-induced band edge displacements and band gap narrowing in 3C–, 4H–, 6H–SiC, and Si," *J. Appl. Phys.*, vol. 84, no. 5, pp. 2628–2637, 1998.

[16] S. C. Jain and D. J. Roulston, "A simple expression for band gap narrowing (BGN) in heavily doped Si, Ge, GaAs and GexSi1−x strained layers," *Solid. State. Electron.*, vol. 34, no. 5, pp. 453–465, May 1991.

[17] L. Patrick and W. J. Choyke, "Static dielectric constant of SiC," *Phys. Rev. B*, vol. 2, no. 6, pp. 2255–2256, 1970.

[18] "Silicon Carbide." [Online]. Available: http://www.ioffe.ru/SVA/NSM/Semicond/SiC. [Accessed: 01-Jan-2017].

[19] M. Ruff, H. Mitlehner, and R. Helbig, "SiC devices: Physics and numerical simulation," *IEEE Trans. Electron Devices*, vol. 41, no. 6, pp. 1040–1054, 1994.

[20] J. B. Casady and R. W. Johnson, "Status of silicon carbide (SiC) as a wide-bandgap semiconductor for high-temperature applications: A review," *Solid. State. Electron.*, vol. 39, no. 10, pp. 1409–1422, 1996.

[21] R. F. Pierret, *Semiconductor Device Fundamentals*. Addison-Wesley Publishing Co., 1996.

[22] D. M. Caughey and R. E. Thomas, "Carrier Mobilities in Silicon Empirically Related to Doping and Field," *Proc. IEEE*, vol. 55, no. 12, pp. 2192–2193, 1967.

[23] M. Roschke and F. Schwierz, "Electron mobility models for 4H, 6H, and 3C SiC," *IEEE Trans. Electron Devices*, vol. 48, no. 7, pp. 1442–1447, 2001.

[24] J. A. Powell, L. G. Matus, and M. A. Kuczmarski, "Growth and Characterization of Cubic SiC Single□Crystal Films on Si," *J. Electrochem. Soc. Solid State Sci. Technol.*, vol. 134, pp. 1558–1565, 1987.

[25] H. Matsuura, Y. Masuda, Y. Chen, and S. Nishino, "Determination of Donor Densities and Donor Levels in 3C-SiC Grown from Si 2 (CH 3) 6 Using Hall-Effect Measurements," *Jpn. J. Appl. Phys.*, vol. 39, no. 9R, p. 5069, 2000.

[26] C. Codreanu, M. Avram, E. Carbunescu, and E. Iliescu, "Comparison of 3C–SiC, 6H–SiC and 4H–SiC MESFETs performances," *Mater. Sci. Semicond. Process.*, vol. 3, pp. 137–142, 2000.

[27] R. P. Joshi and D. K. Ferry, "Calculations of the temperature and field dependent electronic mobility in β-SiC," *Solid. State. Electron.*, vol. 38, no. 11, pp. 1911–1916, 1995.

[28] L. Tirino, M. Weber, K. F. Brennan, E. Bellotti, and M. Goano, "Temperature dependence of the impact ionization coefficients in GaAs, cubic SiC, and zinc-blende GaN," *J. Appl. Phys.*, vol. 94, no. 1, pp. 423–430, 2003.

[29] A. G. Chynoweth, "Ionization Rates for Electrons and Holes in Silicon," *Phys. Rev.*, vol. 109, no. 5, pp. 1537–1540, 1957.

[30] R. Van Overstraeten and H. De Man, "Measurement of the ionization rates in diffused silicon p-n junctions," *Solid State Electron.*, vol. 13, no. 5, pp. 583–608, 1970.

[31] E. Bellotti, H. E. Nilsson, K. F. Brennan, P. P. Ruden, and R. Trew, "Ensemble Monte Carlo calculation of hole transport in bulk 3C–SiC," *J. Appl. Phys.*, vol. 87, 2000.

[32] C. Raynaud, D. Tournier, H. Morel, and D. Planson, "Comparison of high voltage and high temperature performances of wide bandgap semiconductors for vertical power devices," *Diam. Relat. Mater.*, vol. 19, no. 1, pp. 1–6, 2010.

[33] F. C. Beyer, "Deep Levels in SiC," Chemistry and Biology Linkoping University, 2011.

[34] a. a. Lebedev, "Deep level centers in silicon carbide: A review," *Semiconductors*, vol. 33, no. 2, pp. 107–130, 1999.

[35] H. Kuwabara, S. Yamada, and S. Tsunekawa, "Radiative recombination in β-SiC doped with boron," *J. Lumin.*, vol. 12–13, pp. 531–536, Mar. 1976.

[36] H. Kuwabara and S. Yamada, "Free-to-bound transition in β-SiC doped with boron," *Phys. Status Solidi Appl. Mater. Sci.*, vol. 30, no. 2, pp. 739–746, 1975.

[37] H. Kuwabara, K. Yamanaka, and S. Yamada, "Donor-acceptor pair emission from β-sic doped with gallium," *Phys. Status Solidi Appl. Mater. Sci.*, vol. 37, no. 2, pp. 157–161, 1976.

[38] K. F. Dombrowski, U. Kaufmann, M. Kunzer, K. Maier, and J. Schneider, "Deep donor state of vanadium in cubic silicon carbide (3C□SiC)," *Appl. Phys. Lett.*, vol. 65, pp. 1811–1813, 1994.

[39] P. Ščajev, V. Gudelis, K. Jarašiūnas, and P. B. Klein, "Fast and slow carrier recombination transients in highly excited 4H- and 3C-SiC crystals at room temperature," *J. Appl. Phys.*, vol. 108, no. 2, 2010.

[40] G. L. Harris, *Properties of silicon carbide*. London: EMIS Datareviews Series No.13, 1995.

[41] J. Sun *et al.*, "Considerably long carrier lifetimes in high- quality 3C-SiC (111)," *Appl. Phys. Lett.*, vol. 25, 2012.

[42] A. Aditya *et al.*, "Search of appropriate semiconductor for PIN Diode fabrication in terms of resistance analysis," *2015 Int. Conf. Recent Dev. Control. Autom. Power Eng. RDCAPE 2015*, pp. 61–65, 2015.

[43] M. Shur, S. L. Rumyantsev, and M. E. Levinshtein, *SiC Materials and Devices*, no. v. 1. World Scientific, 2006.

978-1-5090-0409-6/17/$31.00 ©2017 IEEE